International Journal for Housing Science and Its Applications
Publish August 10, 2025. Volume 46, Issue 4 Pages 8284-8302

https://doi.org/10.70517/ijhsa464708

Study on the vibration coupling mechanism of a power transmission system with misaligned couplings

Zhao Ji[1,*] and Xia Li[1]
[1] SEW Industrial GEAR (Tianjin) Co., Ltd., Tianjin, 300457, China
Corresponding authors: (e-mail: jidaalang@163.com).

Abstract A dynamic model with bend-torsion coupling was established for helical cylindrical gear split-torque transmission system of heavy load (above 10KNm), in which the time-varying mesh stiffness, random backlash, mesh error and bending deformation of shaft were considered. Express the bending stiffness, the torsional stiffness and the damping coefficients of the dynamic equation using dimension parameters, this model could provide more precise guidance for design work. Acquire the sharing coefficients and the dynamic coefficients, through solving the dynamic equation of system by the fourth-order Runge-Kutta method. The results show that reduction of the diameter of transmission shaft could effective improve the load sharing performance of system; Dynamic factor will fluctuate while the diameter of transmission shaft be smaller than a threshold value; Dynamic coefficients will be reduced while the moment of inertia of the bigger gear on transmission shaft is decreased properly.

Index Terms helical cylindrical gear, dynamic model, sharing coefficients, dynamic coefficients, transmission system

I. Introduction

The helical gear split transmission system achieves torque splitting through a fixed-axis gear train. Compared to planetary gear transmission systems that achieve torque splitting through a floating sun gear, this system offers advantages such as fewer gears and bearings, lower manufacturing costs, and reduced noise. Historically, helical gear split transmission systems have been primarily applied in fields such as helicopters and ships. Due to its higher cost-effectiveness and easier maintenance, the helical gear split transmission system is increasingly being considered as a replacement for existing planetary gear transmission equipment in heavy industries such as mineral processing and steel manufacturing during production line equipment upgrades. Since the helical gear split transmission system lacks the floating structure found in planetary gear transmission systems, effectively addressing the load balancing issue at multiple meshing points becomes critical.

Currently, domestic and international scholars have conducted in-depth research on the dynamic characteristics of cylindrical gear split transmission systems [1]-[16], including studies on the impact of axial lateral displacement on the system's load distribution performance [17]-[25]. However, when the shaft diameter is small, the shaft's bending stiffness is far greater than its torsional stiffness. In the vibration equations, the shaft's bending stiffness has a negligible effect on the system response. Therefore, in these studies, the shaft's torsional stiffness and the system's support stiffness (bearings and housing) are the focus of research, while the influence of the shaft's bending stiffness is ignored. In heavy-duty industrial equipment (10 kNm and above), the shaft diameter and bearing span are generally large, and the bending stiffness and torsional stiffness of the shaft approach the same order of magnitude. The inclusion of shaft bending stiffness enables the system's dynamic response to different shaft diameters to more accurately reflect the effects of various primary and secondary harmonics. In previous studies, a variable control approach was often adopted, neglecting the functional relationship between system damping and system stiffness. Additionally, while some studies considered the meshing clearance function, they overlooked the random nature of gear backlash within tolerance limits. This resulted in the backlash value in the clearance function being treated as a constant, typically selected as the average value of the backlash.

This paper takes a heavy-duty gearbox system under large-scale heavy-duty grinding machine conditions as the research object, considering factors such as the lateral displacement of the shaft caused by shaft bending deformation and support deformation, the functional relationship between damping and corresponding stiffness, time-varying meshing stiffness, and the clearance function under random gear backlash. A system-level bending-torsion coupled dynamic model was established; The study investigates the influence of the comprehensive stiffness of the transmission shaft (using diameter as an indicator), the load distribution coefficient, and the dynamic load coefficient on the system's split stage (first-stage meshing) and parallel stage (second-stage meshing). To provide

a theoretical basis for the design of helical gear split transmission systems, two concepts—engineering load distribution coefficient and engineering dynamic load coefficient—are defined as research objects.

II. Principle of helical gear split transmission system

II. A.Kinetic model

The three-dimensional model of the helical gear split transmission system is shown in Figure 1:

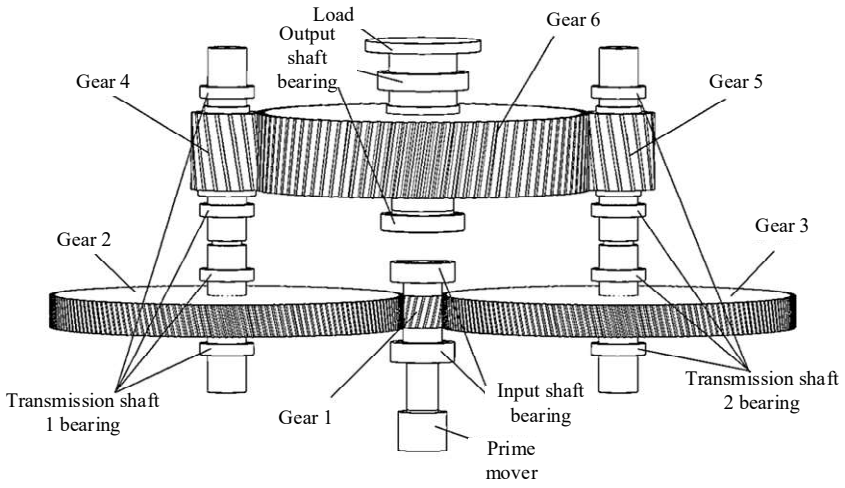

Figure 1: Helical gear split transmission system

The prime mover transmits torque simultaneously to gears 2 and 3 via gear 1 on the input shaft. The shaft connecting gears 2 and 4 is defined as drive shaft 1, and the shaft connecting gears 3 and 5 is defined as drive shaft 2. The final torque is transmitted to gear 6 on the output shaft via gears 4 and 5, driving the load connected to the output shaft.$Z_{11}Z_{11}Z_{11}$

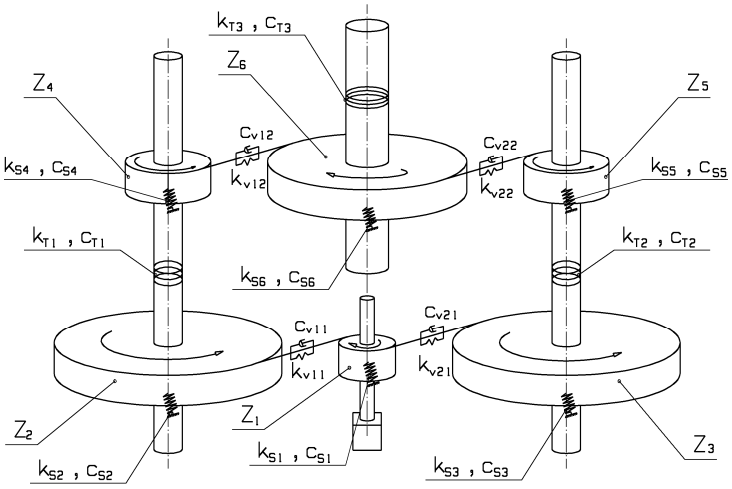

Figure 2: Kinematic model of helical gear split transmission system

The centralized mass method is used to construct the elastic dynamics model of the shunt flow system, as shown in Figure 2. Gear 1,2,3,4,5,6 is defined as Z_1,Z_2,Z_3,Z_4,Z_5, Z_6,m_i(i=1,2,3,4,5,6) are the masses of gear Z_i, r_i (i=1,2,3,4,5,6) are the radius of the base circle of gear Z_i, and J_i(i=1,2,3,4,5,6) are the moment of inertia of gear Z_i, k_{Si}(i=1,2,3,4,5,6) is the shaft bending stiffness corresponding to gear Z_i, c_{Si}(i=1,2,3,4,5,6) is the shaft bending damping coefficient corresponding to gear Z_i, θ_i(i=1,2,3,4,5,6) is the torsional displacement of gear Z_i, and X_i(i=1,2,3,4,5,6) is the displacement of gear Z_i along the tangent of the meshing pair, k_{Ti}(i=0,1,2,3) The torsional stiffness coefficients of the input shaft, the transmission shaft 1, the transmission shaft 2 and the output shaft are respectively, the k_{vi1}(i=1,2) is the time-varying meshing stiffness of Z_1 and Z_2 and Z_3 respectively, the k_{vi2}(i=1,2) is

the time-varying meshing stiffness of Z_6 and Z_4 and Z_5 respectively, and the c_{vi1}(i=1,2) is the meshing damping coefficient of Z_1 and Z_2 and Z_3 respectively , c_{vi2}(i=1,2) is the meshing damping coefficient of Z_6 and Z_4 and Z_5, respectively. J_0, θ_0 is the moment of inertia and torsional displacement of the prime mover; J_7, θ_7 is the moment of inertia and torsional displacement of the load;

The main dynamic parameters of the helical gear split transmission system are shown in Table 1.

Table 1: Main kinetic parameters

Member	Number of teeth	Helical angle	Quality	Moment of inertia	Base radius
		°	kg	$kg \cdot m^2$	m
Prime mover				0.0012	
Gear 1	19	12	154.228	1.94889	0.14564
Gear 2	168	12	11484.405	10806.27697	1.2877635
Gear 3	168	12	11484.405	10806.27697	1.2877635
Gear 4	17	8	901.191	27.51320	0.2255845
Gear 5	17	8	901.191	27.51320	0.2255845
Gear 6	91	8	24117.182	19704	1.19427
Load				836576	

Gear Z_2, Z_3 with a bearing span of 0.4 m on both sides, Gears Z_4 and Z_5 have bearing spans of 0.8 m on both sides, the spans between $Z_2$and Z_4 and between Z_3 and Z_5 are both 1 m.

II. B.Determination of basic parameters

The meshing damping coefficients are

$$c_{vij} = 2\zeta_v \sqrt{\bar{k}_{vij} \frac{r_k^2 r_l^2 J_k J_l}{r_k^2 J_k + r_l^2 J_l}} \tag{1}$$

In the above equation, ζ_v is the meshing damping ratio, and experiments have shown [13] that its value ranges from 0.03 to 0.17. $\bar{k}_{vij}$ (i = 1, 2; j = 1, 2) is the average meshing stiffness of the meshing pair corresponding to the dynamic meshing force F_{ij} (i = 1, 2; j = 1, 2). In this project, $\bar{k}_{v11} = \bar{k}_{v21} = 45 \times 10^8\ N/m$, and $\bar{k}_{v12} = \bar{k}_{v22} = 105.234 \times 10^8\ N/m$. J_k and J_l are the rotational inertias of the two meshing gears, and r_k and r_l are the base circle radii of the two meshing gears.

The torsional damping coefficients of each shaft are

$$c_{Ti} = 2\zeta_T \sqrt{k_{Ti} \frac{J_m J_n}{J_m + J_n}} \tag{2}$$

In the above equation, ζ_T is the torsional damping ratio of the material, and experiments have shown [13] that its value ranges from 0.005 to 0.075. J_m and J_n are the rotational inertias of the two gears on the axis corresponding to the i-th (i = 1, 2, 3, 4) torsional damping. The torsional stiffness can be expressed as

$$k_{Ti} = \frac{G\pi d_i^4}{32 l_{bi}} \tag{3}$$

In the above equation, G is the shear modulus of the material, d_i is the equivalent diameter of the axis corresponding to k_{Ti}, and l_{bi} is the distance between the two gears on the axis corresponding to k_{Ti}.

The bending damping coefficient of each axis is

$$c_{Si} = 2\zeta_S \sqrt{k_{Si} \frac{J_m J_n}{J_m + J_n}} \tag{4}$$

In the above equation, ζ_S is the bending damping ratio of the material, and experiments have shown [13] that its value ranges from 0.03 to 0.1. J_m and J_n are the rotational inertias of the two gears on the axis corresponding to the i-th bending damping.

The bending stiffness of the shaft in this paper is defined as the ratio of the force (meshing force F) acting on the shaft at the gear installation position to the radial deformation w of the shaft at that position. A simplified diagram of the relationship between the radial deformation of the shaft and the meshing force is shown in Figure 3.

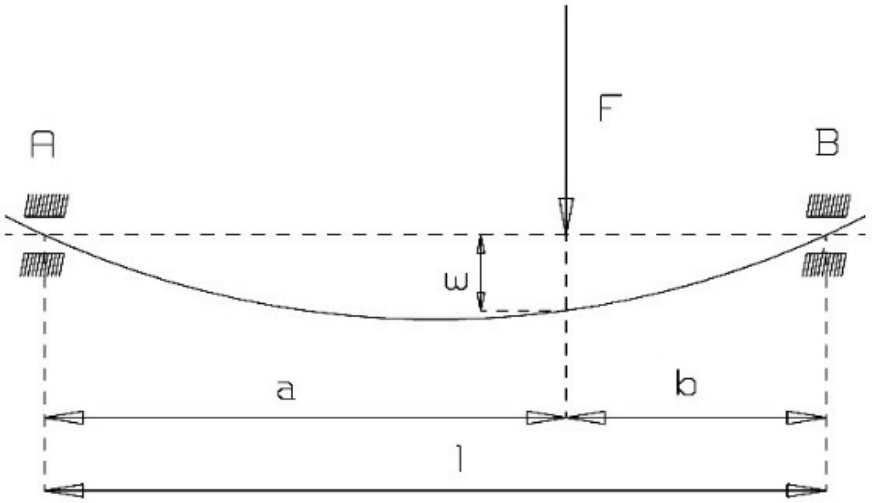

Figure 3: Relationship between radial deformation w of the shaft and meshing force F

In Figure 3, A and B are the bearings on both sides of the gear, l is the span between bearings A and B, the distance between the gear and bearing A is a, and the distance between the gear and bearing B is b. w is the radial deformation of the shaft at the gear installation position. The deformation w can be obtained from formula (5):

$$w = \frac{Fab}{6EIl}(l^2 - a^2 - b^2) \tag{5}$$

In the above equation, E is the elastic modulus of the material, and I is the moment of inertia of the cross section of the shaft relative to the neutral axis.

According to formula (5), the bending stiffness formula of the shaft at the gear mounting location can be obtained:

$$k_{Si} = \frac{F_i}{w_i} = \frac{6EI_i l_i}{a_i b_i (l^2 - a_i^2 - b_i^2)} \tag{6}$$

In the above equation, F_i and w_i represent the meshing force and radial deformation of the shaft at the gear installation position corresponding to the bending damping c_{Si} of the i-th gear, respectively. a_i, b_i, and l_i are the dimensional parameters corresponding to c_{Si} in the tooth-shaft-bearing structure, and I_i is the moment of inertia of the neutral axis of the shaft cross-section corresponding to c_{Si}.

All drive shafts in this paper are circular cross-section shafts, therefore

$$I = \frac{\pi R^4}{4} = \frac{\pi d^4}{64} \tag{7}$$

Expand the time-varying stiffness $k(\mathrm{t})$ using a Fourier series.

$$k(t) = \bar{k}_v + \alpha \sum_{i=1}^{\infty} \sin(i\omega t + \varphi_0) \tag{8}$$

In the above equation, $\bar{k}_v$ is the time-varying meshing stiffness homogeneity, α is the stiffness fluctuation coefficient, ω is the meshing frequency (in this project, the first-order meshing frequency is 235.91667 Hz, and the second-order meshing frequency is 23.885 Hz), and φ_0 is the initial phase.

III. System vibration differential equations and solutions

The differential equations of bending-torsion vibration of the system established according to the Newton-Euler method are as follows:

$$\begin{cases} J_0\ddot{\theta}_0 + c_{\mathrm{T}0}(\dot{\theta}_0 - \dot{\theta}_1) + k_{\mathrm{T}0}(\theta_0 - \theta_1) = T_1 \\ J_1\ddot{\theta}_1 - c_{\mathrm{T}0}(\dot{\theta}_0 - \dot{\theta}_1) - k_{\mathrm{T}0}(\theta_0 - \theta_1) \\ +r_1F_{11}\cos\beta_1 + r_1F_{21}\cos\beta_1 = 0 \\ J_2\ddot{\theta}_2 + c_{\mathrm{T}1}(\dot{\theta}_2 - \dot{\theta}_4) + k_{\mathrm{T}1}(\theta_2 - \theta_4) \\ -r_2F_{11}\cos\beta_1 = 0 \\ J_3\ddot{\theta}_3 + c_{\mathrm{T}2}(\dot{\theta}_3 - \dot{\theta}_5) + k_{\mathrm{T}2}(\theta_3 - \theta_5) \\ -r_3F_{21}\cos\beta_1 = 0 \\ J_4\ddot{\theta}_4 - c_{\mathrm{T}1}(\dot{\theta}_2 - \dot{\theta}_4) - k_{\mathrm{T}1}(\theta_2 - \theta_4) \\ +r_4F_{12}\cos\beta_2 = 0 \\ J_5\ddot{\theta}_5 - c_{\mathrm{T}2}(\dot{\theta}_3 - \dot{\theta}_5) - k_{\mathrm{T}2}(\theta_3 - \theta_5) \\ +r_5F_{22}\cos\beta_2 = 0 \\ J_6\ddot{\theta}_6 + c_{\mathrm{T}3}(\dot{\theta}_6 - \dot{\theta}_7) + k_{\mathrm{T}3}(\theta_6 - \theta_7) \\ -r_6F_{12}\cos\beta_2 - r_6F_{22}\cos\beta_2 = 0 \\ J_7\ddot{\theta}_7 - c_{\mathrm{T}3}(\dot{\theta}_6 - \dot{\theta}_7) - k_{\mathrm{T}3}(\theta_6 - \theta_7) = -T_0 \\ m_1\ddot{X}_1 + c_{S1}\dot{X}_1 + k'_{\mathrm{S}1}X_1 = F_{11} - F_{21} \\ m_2\ddot{X}_2 + c_{S2}\dot{X}_2 + k'_{\mathrm{S}2}X_2 = F_{11} \\ m_3\ddot{X}_3 + c_{S3}\dot{X}_3 + k'_{\mathrm{S}3}X_3 = F_{21} \\ m_4\ddot{X}_4 + c_{S4}\dot{X}_4 + k'_{\mathrm{S}4}X_4 = F_{12} \\ m_5\ddot{X}_5 + c_{S5}\dot{X}_5 + k'_{\mathrm{S}5}X_5 = F_{22} \\ m_6\ddot{X}_6 + c_{S6}\dot{X}_6 + k'_{\mathrm{S}6}X_6 = F_{22} - F_{12} \end{cases} \tag{9}$$

In the above equation, F_{11} and F_{21} are the dynamic meshing forces of the first-level meshing on branch 1 and branch 2, respectively, while F_{12} and F_{22} are the dynamic meshing forces of the second-level meshing on branch 1 and branch 2, respectively. k_{Si} is the equivalent stiffness of k_{Si} and the corresponding bearing stiffness, which can be expressed as

$$k'_{\mathrm{Si}} = \frac{k_{Si} \times k_{\mathrm{C}i}}{k_{Si} + k_{\mathrm{C}i}} \tag{10}$$

In the above equation, k_{Ci} is the bearing support stiffness corresponding to k_{Si}.

Each meshing force can be expressed as

$$\begin{cases} F_{11} = c_{\mathrm{v}11}\dot{Y}_{11} + k_{v11} \cdot f_{11}(Y_{11}) \\ F_{21} = c_{\mathrm{v}21}\dot{Y}_{21} + k_{v21} \cdot f_{21}(Y_{21}) \\ F_{12} = c_{\mathrm{v}12}\dot{Y}_{12} + k_{v12} \cdot f_{12}(Y_{12}) \\ F_{22} = c_{\mathrm{v}22}\dot{Y}_{22} + k_{v22} \cdot f_{22}(Y_{22}) \end{cases} \tag{11}$$

In the above equation, Y_{ij} represents the relative displacement of the meshing line corresponding to the meshing force F_{ij}. At the same time, in order to eliminate the rigid body displacement in the differential equation system (9) while maintaining the topological structure of the system unchanged, it is necessary to convert the torsional displacement of each axle wheel in the system into linear displacement. Y_{ij} can be expressed as:

$$\begin{cases} Y_{11} = (-X_1 + r_1\theta_1) - (r_2\theta_2 + X_2) - e_{11} \\ Y_{21} = (-X_1 + r_1\theta_1) - (r_3\theta_3 + X_3) - e_{21} \\ Y_{12} = (-X_4 + r_4\theta_4) - (r_6\theta_6 + X_6) - e_{12} \\ Y_{22} = (-X_5 + r_5\theta_5) - (r_6\theta_6 + X_6) - e_{22} \end{cases} \tag{12}$$

In equation (12), e_{ij} is the meshing error corresponding to F_{ij}.

In equation (11), $f_{ij}(Y_{ij})$ is the clearance function of the gear meshing pair. Let the meshing clearance be $2b_{ij}$, where b_{ij} is half of the tooth side clearance of the jth branch of the ith meshing stage. Then, $f_{ij}(Y_{ij})$ can be expressed as:

$$f_{\mathrm{ij}}(Y_{\mathrm{ij}}) = \begin{cases} Y_{\mathrm{ij}} - b_{ij} & Y_{\mathrm{ij}} > b_{ij} \\ 0 & -b_{ij} \le Y_{\mathrm{ij}} \le b_{ij} \\ Y_{\mathrm{ij}} + b_{ij} & Y_{\mathrm{ij}} < -b_{ij} \end{cases} \tag{13}$$

In this project, the gear machining accuracy is 5 grades, and for the first-level meshing of the system, 3192 rational numbers are randomly selected according to the normal distribution between the b_{11} and the b_{12} between 0.522 mm~0.851 mm respectively to generate a periodic piecewise function about time t. For the secondary

meshing of the system, 1530 rational numbers were randomly selected from the b_{12} and b_{22} according to the normal distribution between 0.523 mm~0.853 mm to generate a periodic piecewise function about time t. Take $b_{11}(\mathrm{t})$ as an example, in the form of this

$$b_{11}(t)=\begin{cases}0.513 & 0\le t<t_{\mathrm{h}}\\ \ldots & \ldots\\ 0.639 & 3191t_{\mathrm{h}}\le t<3192t_{\mathrm{h}}\\ b_{11}(t-T) & t\ge 3192t_{\mathrm{h}}\end{cases} \tag{14}$$

In equation (14), $t_{\mathrm{h}}=0042388$ (s) is the duration of a single engagement, and $T=3192t_{\mathrm{h}}$ is a full engagement cycle.

IV. Solving systems of differential equations of dynamics

Using formulas (1), (2), (3), (4), and (6), along with knowledge of materials mechanics, transform the coefficients of the system of differential equations (9) into expressions in terms of d_i. Combine formulas (7), (10), (11), and (12) with the system of differential equations (9), and solve using the 4th-order Runge-Kutta method. The mathematical solution process is as follows:

Since the system of equations (9) is a 14-variable second-order differential equation system, it cannot be directly solved using the Runge-Kutta method. Therefore, $u_{\mathrm{i}}=\frac{dy_{\mathrm{i}}}{dx}$ is introduced to transform the system of equations (9) into a 28-variable first-order differential equation.

For convenience of calculation, the unknown quantities are uniformly replaced, and only the matrix is changed as shown in formula (15):

$$\begin{bmatrix}y_0\\ y_1\\ y_2\\ y_3\\ y_4\\ y_5\\ y_6\\ y_7\\ y_8\\ y_9\\ y_{10}\\ y_{11}\\ y_{12}\\ y_{13}\end{bmatrix}=\begin{bmatrix}\theta_0\\ \theta_1\\ \theta_2\\ \theta_3\\ \theta_4\\ \theta_5\\ \theta_6\\ \theta_7\\ X_1\\ X_2\\ X_3\\ X_4\\ X_5\\ X_6\end{bmatrix} \tag{15}$$

Now, using formula (15) and the introduced unknown quantity u_i, equation (9) is transformed as follows:

$$
\begin{cases}
J_0\dot{u}_0 + c_{T0}(u_0 - u_1) + k_{T0}(y_0 - y_1) = T_1 \\
J_1\dot{u}_1 - c_{T0}(u_0 - u_1) - k_{T0}(y_0 - y_1) \\
+r_1F_{11}\cos\beta_1 + r_1F_{21}\cos\beta_1 = 0 \\
J_2\dot{u}_2 + c_{T1}(u_2 - u_4) + k_{T1}(y_2 - y_4) \\
-r_2F_{11}\cos\beta_1 = 0 \\
J_3\dot{u}_3 + c_{T2}(u_3 - u_5) + k_{T2}(y_3 - y_5) \\
-r_3F_{21}\cos\beta_1 = 0 \\
J_4\dot{u}_4 - c_{T1}(u_2 - u_4) - k_{T1}(y_2 - y_4) \\
+r_4F_{12}\cos\beta_2 = 0 \\
J_5\dot{u}_5 - c_{T2}(u_3 - u_5) - k_{T2}(y_3 - y_5) \\
+r_5F_{22}\cos\beta_2 = 0 \\
J_6\dot{u}_6 + c_{T3}(u_6 - u_7) + k_{T3}(y_6 - y_7) \\
-r_6F_{12}\cos\beta_2 - r_6F_{22}\cos\beta_2 = 0 \\
J_7\dot{u}_7 - c_{T3}(u_6 - u_7) - k_{T3}(y_6 - y_7) = -T_0 \\
m_1\dot{u}_8 + c_{S1}u_8 + k'_{S1}y_8 = F_{11} - F_{21} \\
m_2\dot{u}_9 + c_{S2}u_9 + k'_{S2}y_9 = F_{11} \\
m_3\dot{u}_{10} + c_{S3}u_{10} + k'_{S3}y_{10} = F_{21} \\
m_4\dot{u}_{11} + c_{S4}u_{11} + k'_{S4}y_{11} = F_{12} \\
m_5\dot{u}_{12} + c_{S5}u_{12} + k'_{S5}y_{12} = F_{22} \\
m_6\dot{u}_{13} + c_{S6}u_{13} + k'_{S6}y_{13} = F_{22} - F_{12} \\
u_0 = \dot{y}_0 \\
u_1 = \dot{y}_1 \\
u_2 = \dot{y}_2 \\
u_3 = \dot{y}_3 \\
u_4 = \dot{y}_4 \\
u_5 = \dot{y}_5 \\
u_6 = \dot{y}_6 \\
u_7 = \dot{y}_7 \\
u_8 = \dot{X}_1 \\
u_9 = \dot{X}_2 \\
u_{10} = \dot{X}_3 \\
u_{11} = \dot{X}_4 \\
u_{12} = \dot{X}_5 \\
u_{13} = \dot{X}_6
\end{cases}
\tag{16}
$$

Then, the 4th-order Runge-Kutta numerical integration is

$$
\begin{cases}
y_{n+1} = y_n + \lambda_0(K_1 + 2K_2 + 3K_3 + K_4)/6 \\
u_{n+1} = y_n + \lambda_0(q_1 + 2q_2 + 3q_3 + q_4)/6
\end{cases}
\tag{17}
$$

In system of equations (17):

$K_1 = f(x_n, y_n, u_n)$
$K_2 = f(x_n + \lambda_0/2, y_n + \lambda_0 K_1/2, u_n + \lambda_0 q_1/2)$
$K_3 = f(x_n + \lambda_0/2, y_n + \lambda_0 K_2/2, u_n + \lambda_0 q_2/2)$
$K_4 = f(x_n + \lambda_0/2, y_n + \lambda_0 K_3/2, u_n + \lambda_0 q_3/2)$
$q_1 = v(x_n, y_n, u_n)$
$q_2 = v(x_n + \lambda_0/2, y_n + \lambda_0 K_1/2, u_n + \lambda_0 q_1/2)$
$q_3 = v(x_n + \lambda_0/2, y_n + \lambda_0 K_2/2, u_n + \lambda_0 q_2/2)$
$q_4 = v(x_n + \lambda_0/2, y_n + \lambda_0 K_3/2, u_n + \lambda_0 q_3/2)$

In equation (16), λ_0 is the integration step size selected for the calculation. When x $= x_0$, y$= y_0$, and $u = u_0$, according to the above formula, the system of differential equations can be solved starting from (x_0, y_0).

IV. A. Dynamic uniform load coefficient and engineering uniform load coefficient

In equation set (9), the target unknown quantities are the torsional displacement and radial displacement of the gear. Since there are many unknown quantities to be solved, only some of the calculation results for a drive shaft diameter of 360 mm are shown here: radial displacement X_3 is shown in Figure 4, radial displacement X_5 is shown in Figure 5, and rotational speed $\dot{\theta_2}$ is shown in Figure 6.

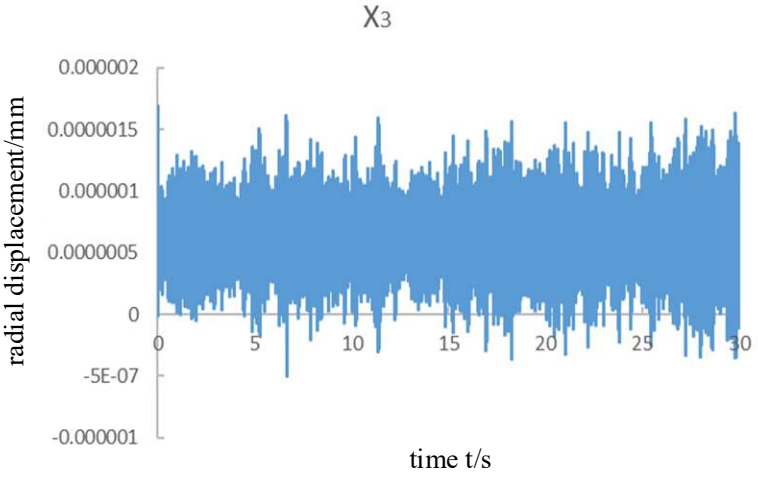

Figure 4: Radial displacement X_3

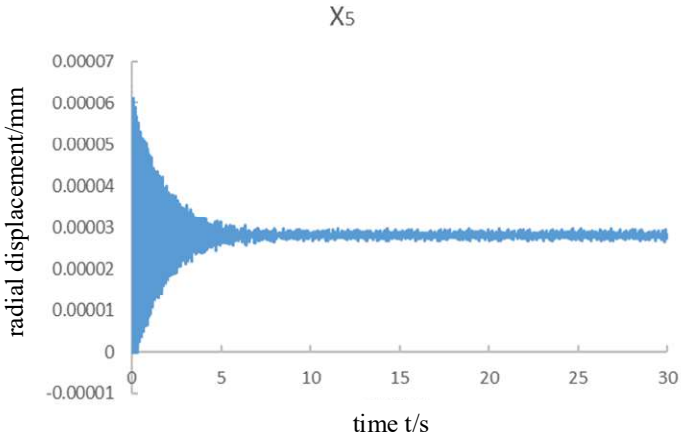

Figure 5: Radial displacement X_5

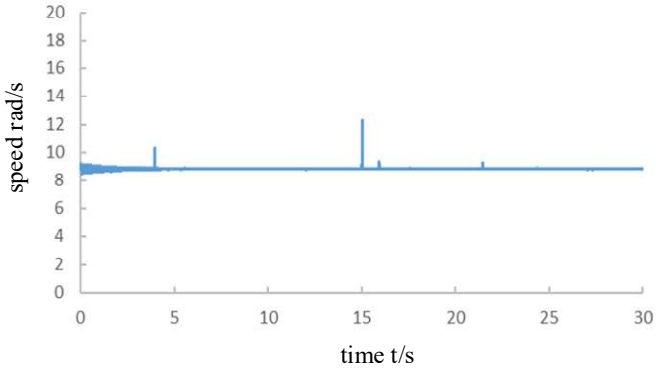

Figure 6: Rotational speed $\dot{\theta_2}$

In engineering problems, changes in meshing forces warrant further investigation. This requires substituting the solutions of the differential equation system into formula (10) to calculate the dynamic meshing forces F_{11}, F_{21}, F_{12}, and F_{22}. Taking the dynamic meshing forces at a shaft diameter of 200 mm as an example, the results are shown in Figures 7–10:

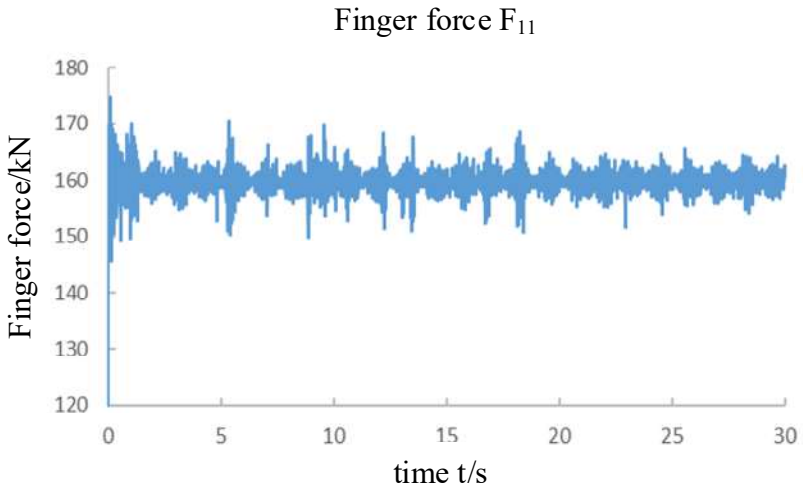

Figure 7: Engagement force F_{11} at $d = 200\ mm$

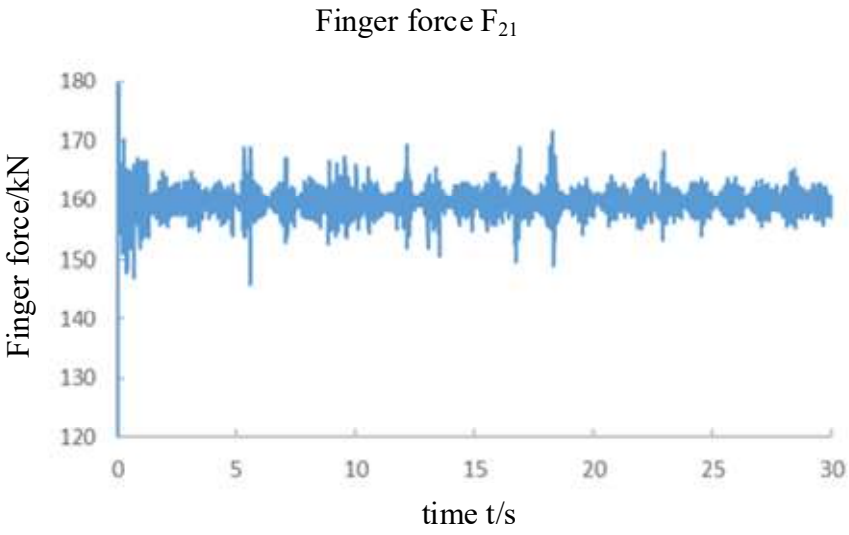

Figure 8: Engagement force F_{21} at $d = 200\ mm$

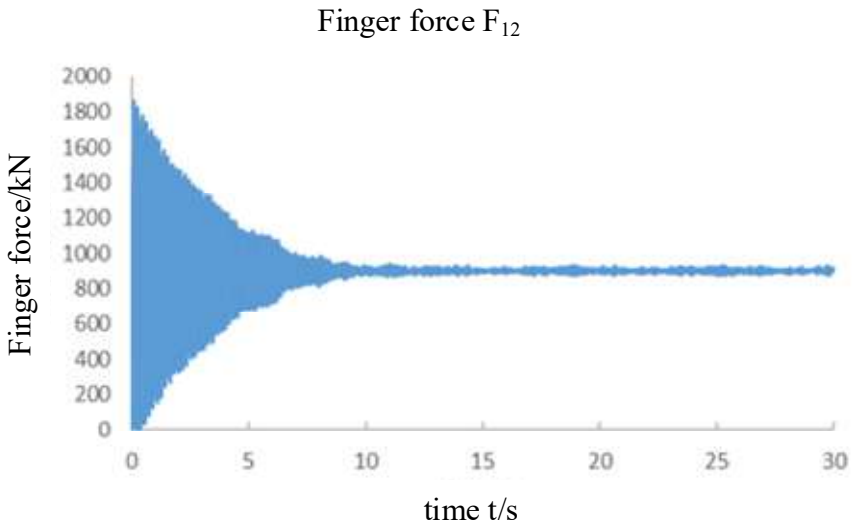

Figure 9: Engagement force F_{12} at $d = 200\,mm$

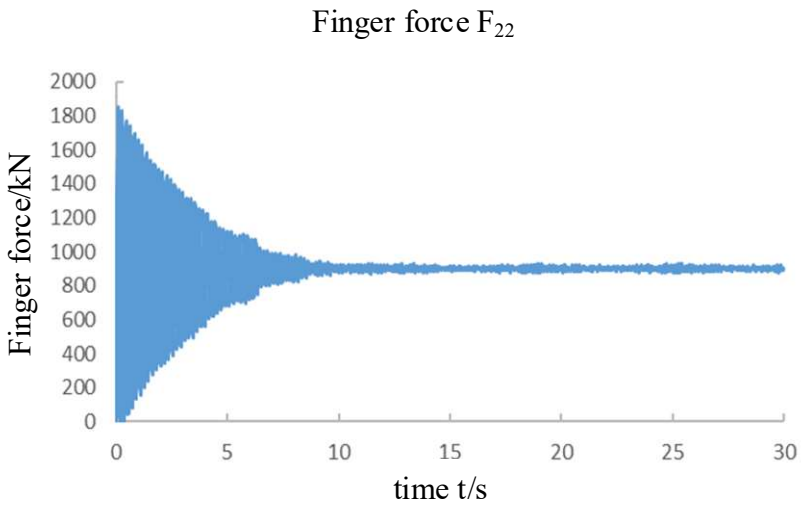

Figure 10: Engagement force F_{22} at $d = 200\,mm$

By comparing Figures 7 and 8 with Figures 9 and 10, it can be seen that the time required for secondary meshing to reach stability is much longer than that for primary meshing.

The dynamic load distribution coefficient is defined as follows:

$$\begin{cases} g_1 = 2 \times (F_{11}, F_{21})_{max} / (F_{11} + F_{21}) \\ g_2 = 2 \times (F_{12}, F_{22})_{max} / (F_{12} + F_{22}) \end{cases} \tag{18}$$

g_1 and g_2 are the dynamic load distribution coefficients for the first-stage and second-stage meshing, respectively. These coefficients reflect the dynamic load distribution of different branches within the same meshing stage of the helical gear flow-sharing system. Below, we use the load distribution coefficients for the first and second stages of meshing when the shaft diameter $d = 200mm$, $d = 250mm$, and $d = 300mm$ as examples. The changes in the load distribution coefficients over time are shown in Figures 11 to 16, respectively.

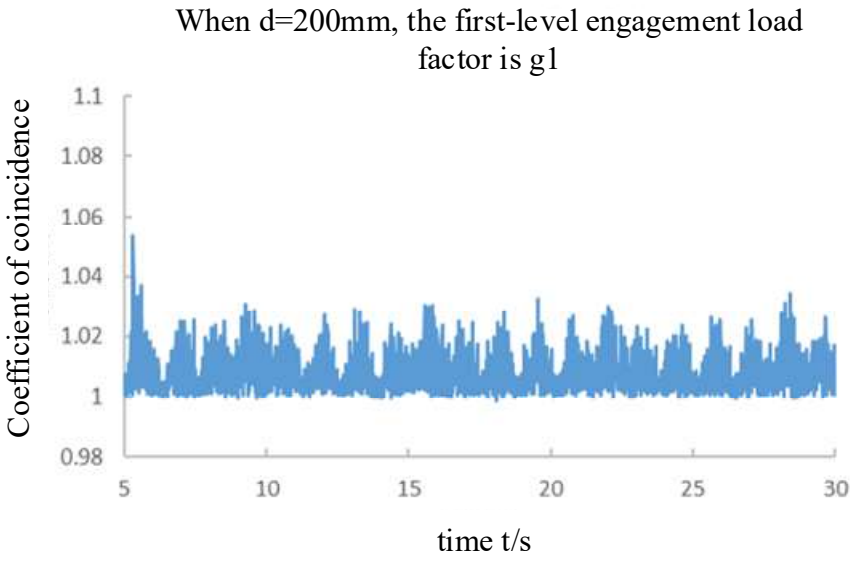

Figure 11: $d = 200\ mm$ First-stage meshing dynamic load distribution coefficient

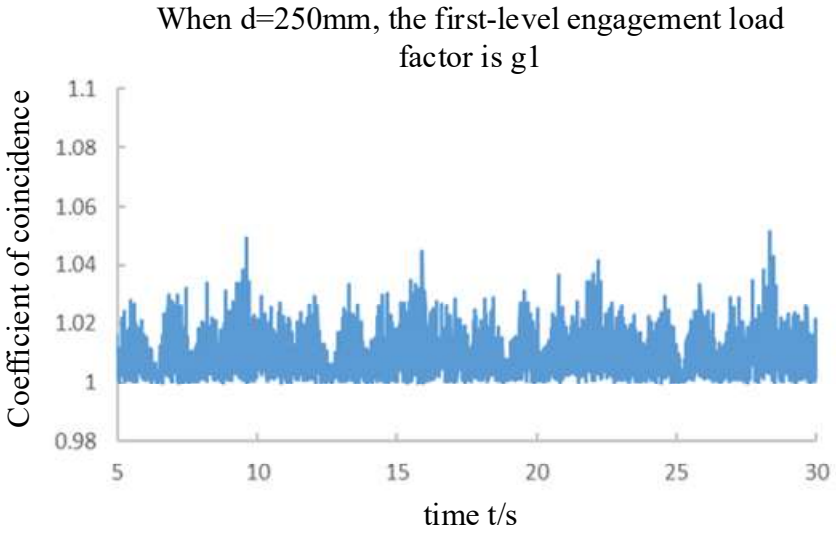

Figure 12: $d = 250\ mm$ First-stage meshing dynamic load distribution coefficient

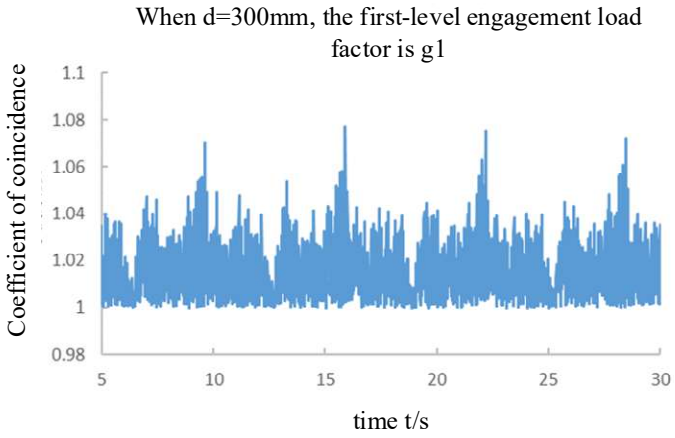

Figure 13: $d = 300\ mm$ First-stage meshing dynamic load distribution coefficient

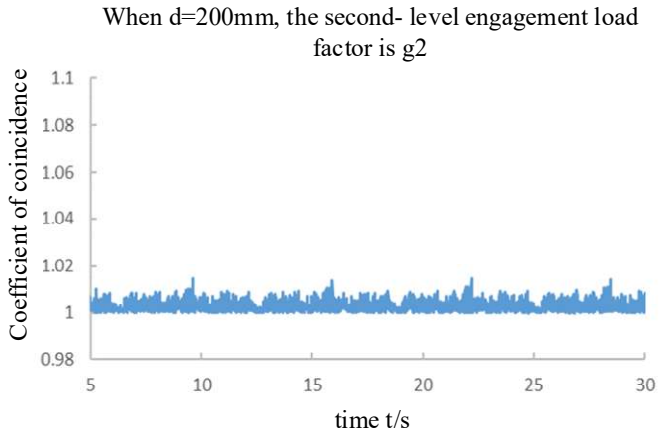

Figure 14: $d = 200\ mm$ Second-stage meshing dynamic load distribution coefficient

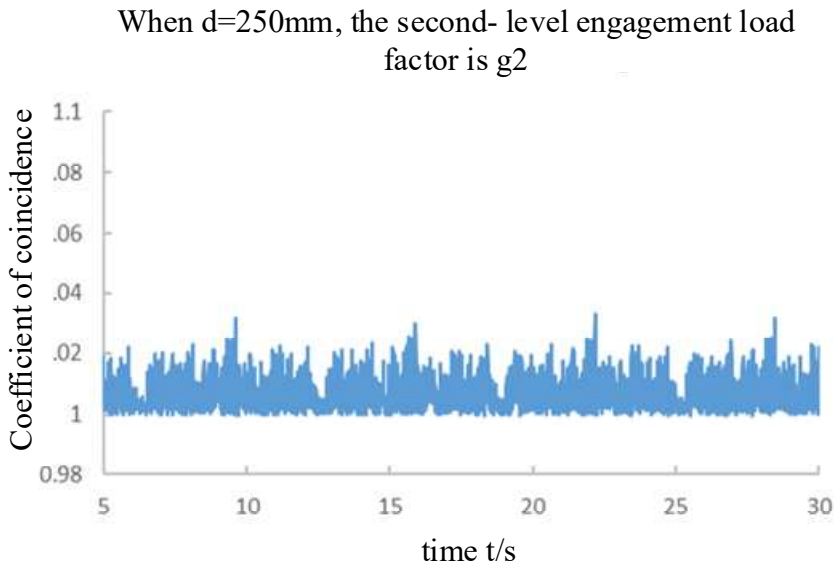

Figure 15: $d = 250\ mm$ Second-stage meshing dynamic load distribution coefficient

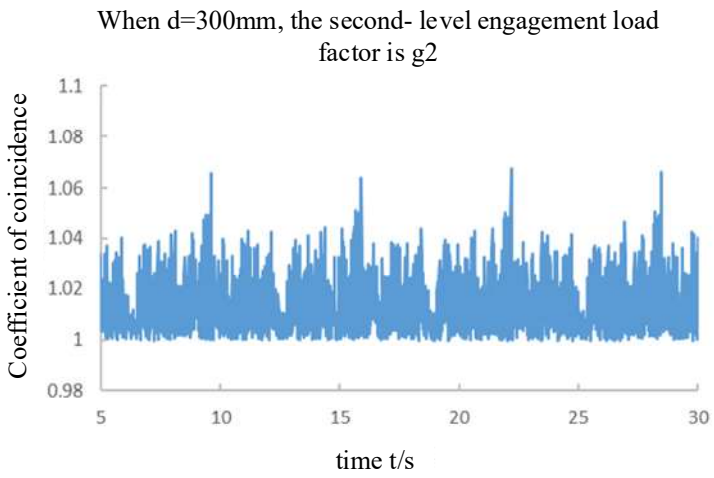

Figure 16: $d = 300\ mm$ Second-stage meshing dynamic load distribution coefficient

As shown in the figure, due to the fact that the tooth side clearance between Branch 1 and Branch 2 reaches its maximum difference at regular intervals, the corresponding dynamic load distribution coefficient also reaches its peak value. Although the average values of the dynamic load distribution coefficient vary little across different shaft diameters, the periodic peaks exhibit significant differences. For the design of transmission systems, these periodically occurring peaks hold greater practical engineering significance.

The average value of the periodic peak of the dynamic load distribution coefficient is defined as the engineering load distribution coefficient. g_{1t} and g_{2t} are defined as the engineering load distribution coefficients for the first-stage meshing and second-stage meshing, respectively.

IV. B. Dynamic live load coefficient and engineering live load coefficient

The load distribution coefficient can only express the load distribution situation of shunting and parallel operation, but it cannot express the changes in dynamic forces. The dynamic load coefficient is defined as follows:

$$\begin{cases} G_1 = (F_{11}, F_{21})_{max}/F_{01} \\ G_2 = (F_{12}, F_{22})_{max}/F_{02} \end{cases} \tag{19}$$

In the above equation, G_1 and G_2 represent the dynamic load coefficients for the first and second stages of meshing, respectively, while F_{01} and F_{02} represent the theoretical meshing forces for the first and second stages of meshing, respectively. Below, we take the dynamic load factors for the first and second stages of meshing as examples when the shaft diameter of the drive shaft is $d = 200mm$, $d = 250mm$, and $d = 300mm$. The changes in the dynamic load factors over time are shown in Figures 17 to 22, respectively.

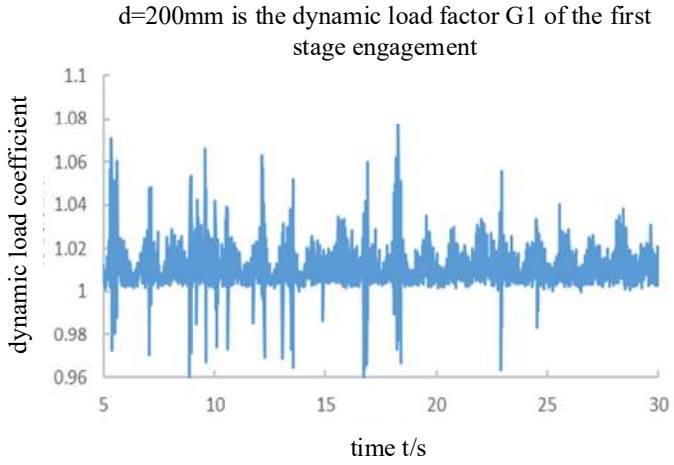

Figure 17: $d = 200\ mm$ First-stage meshing dynamic load factor

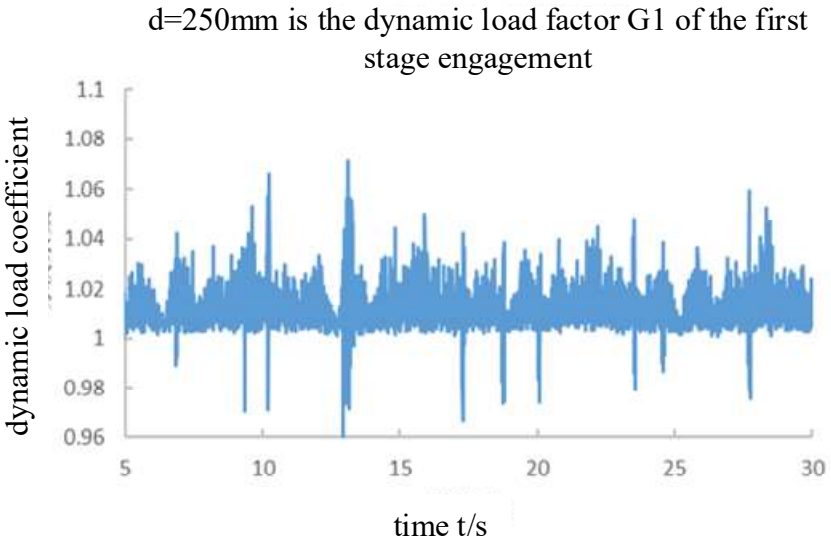

Figure 18: $d = 250\ mm$ First-stage meshing dynamic load factor

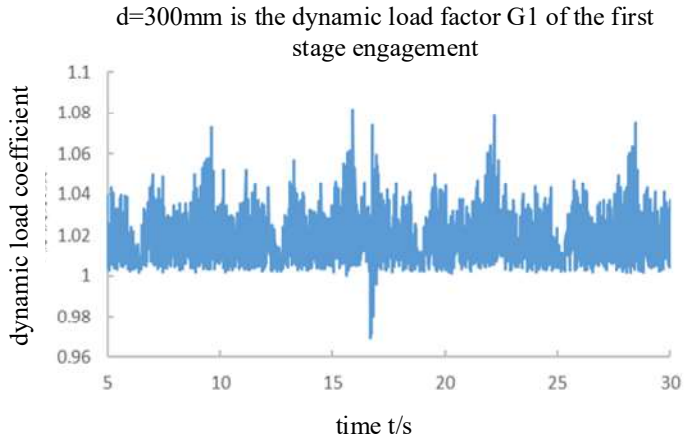

Figure 19: $d = 300\ mm$ First-stage meshing dynamic load factor

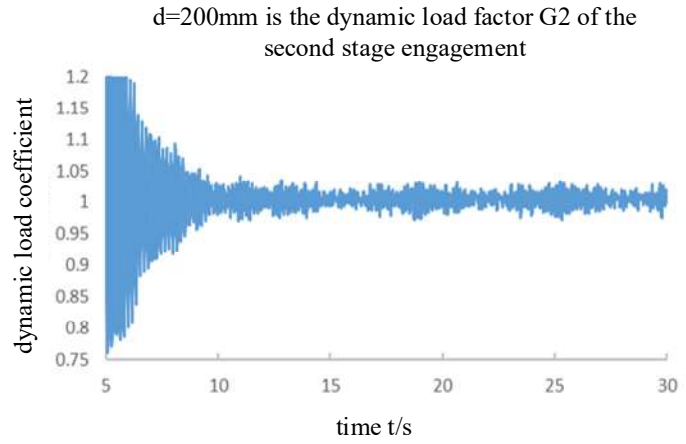

Figure 20: $d = 200\ mm$ Second-stage meshing dynamic load factor

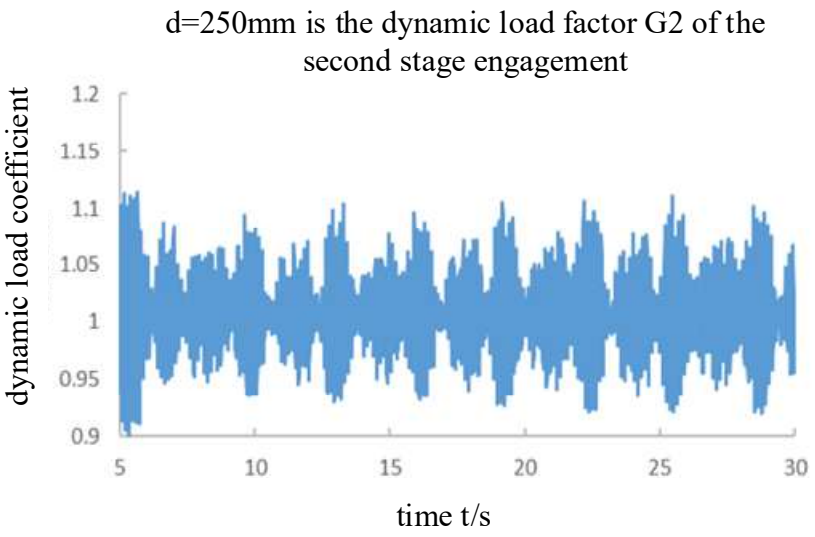

Figure 21: $d = 250\ mm$ Second-stage meshing dynamic load factor

As shown in Figures 20–22, when the shaft diameter of the drive shaft is small, the helical gear split transmission system takes longer to stabilize from startup. This is because the bending damping c_{Si} and torsional damping $c_{\mathrm{T}i}$ are directly proportional to their corresponding structural stiffness k_{Si} and $k_{\mathrm{T}i}$. As shown in equations (3) and (6), the structural stiffness k_{Si} and $k_{\mathrm{T}i}$ are directly proportional to the shaft diameter.

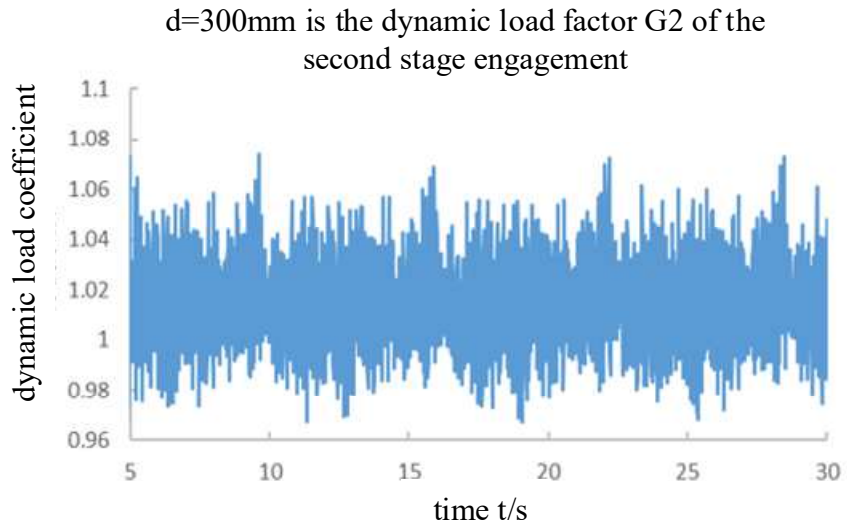

Figure 22: $d = 300\ mm$ Second-stage meshing dynamic load factor

As shown in Figures 17 to 22, the dynamic dynamic load coefficient is similar to the dynamic average load coefficient in that the average values of the dynamic dynamic load coefficient do not vary significantly across different shaft diameters, but the periodic peak values exhibit significant differences.

The average value of the periodic peaks of the dynamic dynamic load coefficient is defined as the engineering dynamic load coefficient. $G_{1\mathrm{t}}$ and $G_{2\mathrm{t}}$ are defined as the engineering dynamic load coefficients for the first and second stages of meshing, respectively.

IV. C. Effect of drive shaft diameter d on engineering load distribution coefficient

Since the diameter d of the drive shaft simultaneously affects both the bending stiffness and torsional stiffness of the shaft, it is more practical to study the relationship between the shaft diameter d and the engineering load distribution coefficients g_{1t} and g_{2t} using d as the variable. The shaft diameter is selected within the range of 130 mm to 400 mm. Each simulation lasts 30 seconds. The data is read from the point when the system stabilizes (8 seconds for shaft diameters less than 200 mm, and 5 seconds for others) until the end of the simulation. The g_{1t} and g_{2t} values for each simulation are recorded, and the g_{1t}/g_{2t}-d relationship curve is plotted as shown in Figure 23.

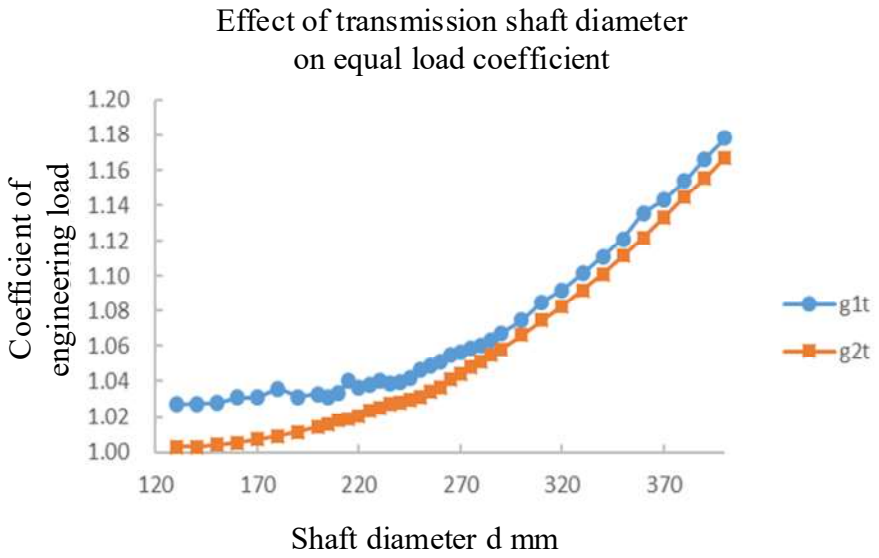

Figure 23: Effect of shaft diameter d on engineering uniform load coefficients g_{1t} and g_{2t}

As shown in Figure 23, in this project, the relationship between the two-stage load distribution coefficient and the shaft diameter can be fitted into a fourth-order polynomial, with a goodness-of-fit $R^2 \geq 0.998$. When the shaft diameter d< 150 mm, the load distribution coefficient changes slowly. It can be seen that within a certain range, reducing the shaft diameter d can effectively improve the load distribution coefficient.

IV. D. Effect of drive shaft diameter d on engineering dynamic load coefficient

Taking the engineering dynamic load coefficients G_{1t} and G_{2t} as the observation objects, this study investigates the relationship between the shaft diameter d and the engineering dynamic load coefficients. The simulation grouping, duration, and data reading methods are the same as those in Section 3.3. The G_{1t}/G_{2t}-d relationship curve is shown in Figure 24.

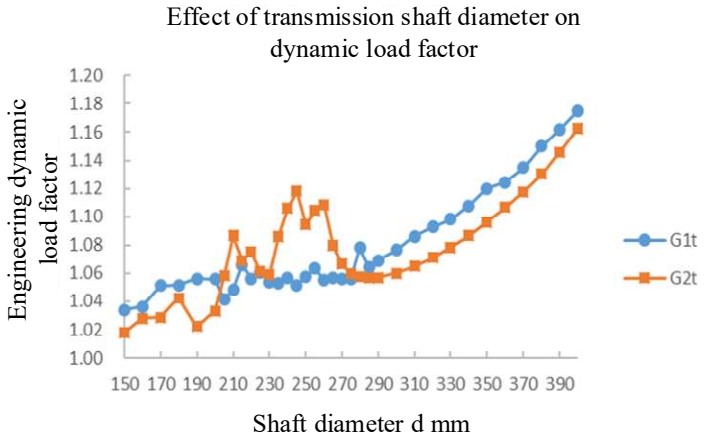

Figure 24: Effect of shaft diameter d on engineering dynamic load coefficients G_{1t} and G_{2t}

As shown in Figure 24, when the shaft diameter d is less than 280 mm, the trend of the engineering dynamic load coefficient exhibits significant fluctuations. At this point, further reducing the shaft diameter will not improve the meshing condition. This is due to the combined effects of the primary and secondary resonances of the shaft's bending-torsion behavior.

To investigate the influence of the bending stiffness and torsional stiffness of the drive shaft on the fluctuations in the engineering dynamic load coefficient, a bending-torsion model is established that only considers the deformation of the shaft support. The model is established in the same manner as described earlier, but the influence of the shaft bending stiffness is excluded. The relationship between the shaft diameter d and the dynamic load coefficient is shown in Figure 25.

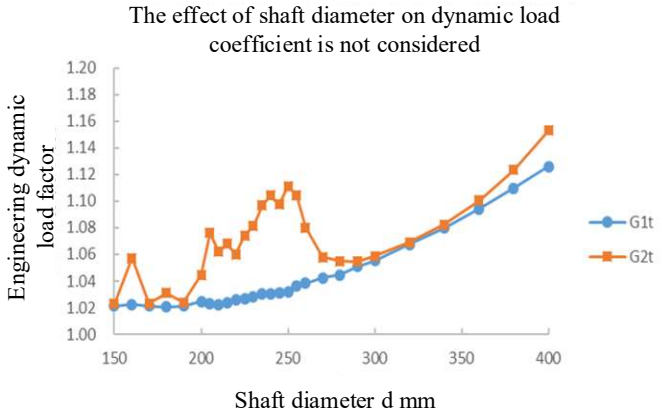

Figure 25: Bending-torsion model G_{1t}/G_{2t}-d without considering shaft bending deformation

As shown in Figure 25, when the bending deformation of the drive shaft is not considered, the peak value of the curve G_{2t}-d and its corresponding diameter are slightly different from those when the bending deformation of the drive shaft is considered, but the overall trend is similar; while the curve G_{1t}-d becomes smoother than when the bending deformation of the drive shaft is considered. It can be seen that the bending deformation of the drive shaft has a greater impact on the engineering dynamic load coefficient G_{1t} of the first-stage meshing.

IV. E. Effect of rotational inertia on engineering dynamic load coefficient

By comparing Figures 24 and 25, it can be seen that the primary cause of fluctuations in the trend diagram of the engineering dynamic load coefficient G_{2t}-d is torsional vibration. Since the force conditions of gears Z_2 and Z_3 are better than those of other gears, and their larger diameters allow for a significant change in their rotational inertia by removing a small amount of mass without significantly affecting their strength. Next, we consider altering the rotational inertia J_2 of gears Z_2 and Z_3 by machining concentric circular grooves on their end faces, thereby modifying the natural frequency of the torsional system. The G_{2t}-d trend under different J_2 values is shown in Figure 26.

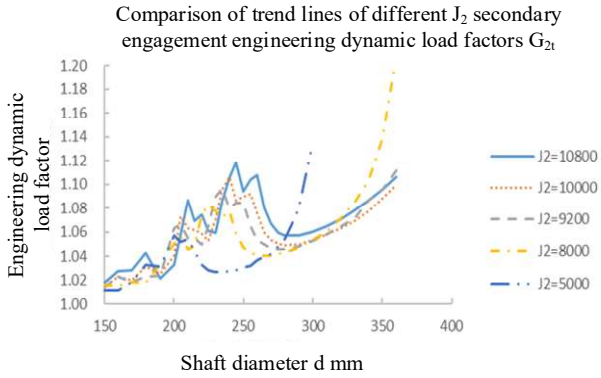

Figure 26: G_{2t}-d trend diagram under different J_2 conditions

As shown in Figure 26, as J_2 decreases, the G_2-d trend line gradually shifts to the left, and the amplitude of the peaks gradually decreases. In this project, due to the root circle constraints of Z_4 and Z_5 the shaft diameter of the drive shaft is approximately 285 mm. Appropriately reducing J_2 can effectively improve the dynamic load coefficient G_2: in this project, reducing J_2 by 6% is sufficient to control the dynamic load coefficient G_2 within 1.05.

Using the same method, the G_{1t}-d trend under different J_2 values is shown in Figure 27.

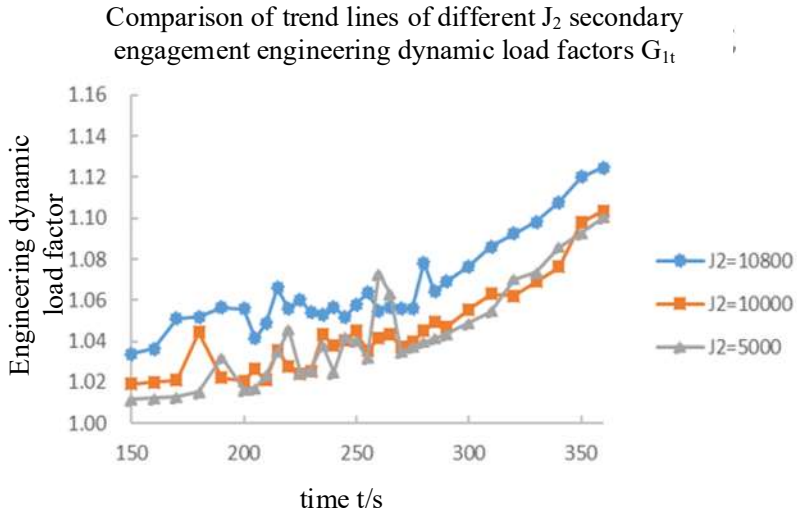

Figure 27: G_{1t}-d trend diagram under different J_2 conditions

As can be seen from Figure 27, changing J_2 has little effect on the engineering dynamic load coefficient of the first-stage meshing, and when J_2 is significantly reduced, there is a tendency for the peak value to shift to the right. Therefore, considering only the first-stage meshing, it is not advisable to reduce J_2 too much.

V. Conclusion

(1) By establishing the nonlinear vibration differential equation system for the split-drive transmission system, which incorporates the functions of shaft bending deformation, bearing deformation, shaft torsional deformation, damping, and corresponding stiffness, we have modeled the system's dynamic response. Comparing Figures 25 and 26, it is evident that under heavy-load conditions (where the drive shaft diameter is larger), the vibration differential equation system that accounts for shaft bending deformation more accurately reflects the system's dynamic response.

(2) Within a certain range, reducing the shaft diameter d can effectively improve the engineering load distribution coefficient. The g_{it}-d (i=1,2) curve can be fitted into a fourth-order polynomial. Therefore, when the shaft diameter d is less than a certain threshold, further reducing the shaft diameter d has a negligible effect on improving the engineering load distribution coefficient. Considering that the stress limits of components in engineering practice are more critical than the system's load distribution, it is not advisable to indiscriminately reduce the shaft diameter d solely to improve the system's load distribution.

(3) When the drive shaft diameter d is below a certain threshold, the engineering dynamic load coefficient exhibits significant fluctuations. When design parameters are far above this threshold, reducing the shaft diameter d can effectively improve the dynamic load state. However, once the design parameters approach or fall below this threshold, reducing the shaft diameter d becomes meaningless.

(4) Within this range, appropriately reducing the rotational inertia of the larger gear on the drive shaft can effectively lower the system's engineering dynamic load coefficient. This is primarily because, in this system, due to the large single-stage transmission ratio, the diameter of the larger gear on the drive shaft is much larger than the shaft diameter, resulting in a lower torsional natural frequency. When the shaft diameter d remains unchanged, reducing the rotational inertia of this gear can effectively alter the system's natural frequency.

(5) Since reducing the rotational inertia of the larger gear on the drive shaft shifts the G_i-d curve to the left overall, the rotational inertia of this gear should not be reduced excessively. In this project, a 6% reduction is sufficient to effectively improve the system's dynamic load coefficient.

References

[1] WHITE G. Design study of a 375 kW helicopter transmission with split-torque epicyclic and bevel drive stages[J]. Journal of Mechanical Engineering Science,1983,197(4) :213-224.

[2] WHITE G. Split torque helicopter transmissions with widely separated engines[J] . Journal of Aerospace Engineering, 1989, 203(1) :53-65.

[3] YANG Zhen, WANG Sanmin, FAN Yesen. Nonlinear dynamic characteristics of split-torque gear transmission system[J]. Journal of Mechanical Engineering, 2008, 44(7):52-57.

[4] WHITE G. 3600 Hp split torque helicopter transmission [R] . Cleveland:NASA CR-174932, 1985,:1-2.

[5] Zhonghong Bu,Geng Liu,Liyan Wu.Modal analyses of herringbone planetary gear train with journal bearings[J].Mechanism and Machine Theory, 2012(54):99-115.

[6] WHITE G. Design study of a split torque helicopter transmission[J]. Journal of Mechanical Engineering, 1998, 212(2):117-123.

[7] M.Ajmi and P.Velex,A Model for Simulating the Quasi-Static and Dynamic Behavior of Double Helical Gears[J].Mechanism and Machine Theory,2005(40): 173-190.

[8] Sondkar Prashant.Dynamic modeling of double-helical planetary gear sets[D]. Ohio:The Ohio State University,2012.

[9] BODAS A,KAHRAMAN A.Influence of carrier and gear manufac- turing errors on the static load sharing behavior of planetary gear sets[J].JSME International Journal Series C,Mechanical Systems,Ma- chine Elements and Manufacturing,2004,47(3):908-915

[10] Wei Jing,Yang Panwu,Qin Datong,Zhang Aiqiang,Bai Peixin.Load sharing characteristics of the herringbone star gear transmission system with flexible pin [J]. Journal of HARBIN INSTITUTE of Technology, 2018,50(07):144-153.

[11] MA P,BOTMAN M.Load sharing in a planetary gear stage in the presence of gear errors and misalignment[J].Journal of Mechanisms,Transmissions,and Automation in Design,1985,107(1): 4-10.

[12] SINGH A.Application of a system level model to study the planetary load sharing behavior[J].Journal of Mechanical Design,2005,127 (3)

[13] ZHU C C,XU X Y,LIU H J,et al.Research on dynamical characteristics of wind turbine gearboxes with flexible pins[J].Renewable Energy,2014,68(7)

[14] DONG Hao, FANG Zongde, WANG Baobin, et al. Load-sharing characteristics of gear train with dual power split based on deflection compatibility[J]. Journal of South China University of Technology, 2012,40(5):18-22.

[15] Wei Jing,Zhang Daqiang,QinDatong,et al.Coupling vibration analysis for planetary gear system considering flexible structure[J]. Journal of Mechanical Engineering, ,2017,53(1):1-12.

[16] ZHU Weilin,WU Shijing,WANG Xiaosun,et al.Influence of posi- tion errors on the load-sharing characteristics of compound planetary gear sets considering the variable stiffness coefficient[J].Journal of Vibration and Shock,2016,35(12):77-85.

[17] CHANG Lehao.A generalized dynamic model for parallel shaft gear transmissions and the influences of dynamic excitations[D].Xi'an:Northwest Polytechnical University,2014

[18] YUAN Qingyu,ZHU Rupeng,ZHU Zibing,et al.Analysis of static load sharing in a 2-stage star gearing system[J].Mechanical Science and Technology,2004,23(7):789-792

[19] TAN Yuanqiang,HU Congfang,ZHANG Yuechun,et al.Testing research on dynamic load sharing performance of encased differential planetary gearbox[J].Journal of Mechanical Engineering,2016,52 (9):28-35.

[20] ZHU Weilin,WU Shijing,WANG Xiaosun,et al.Influence of posi- tion errors on the load-sharing characteristics of compound planetary gear sets considering the variable stiffness coefficient[J].Journal of Vibration and Shock,2016,35(12):77-85.

[21] Du Jinfu,Fang Zongde,Wang Baobin,et al.Study on load sharing behavior of planetary gear train based on deformation compatibility[J]. Journal of AerospacePower,2012,27(5):1166-1171.

[22] LIN H H, Huston R L, Coy J J. On dynamic loads in parallel shaft transmissions[J]. Journal of Mechanisms,Transmissions andAutomation in Design, 1987, 110(2):221-229.

[23] GMIRYA Y. Multi-path rotary wing aircraft gearbox: US7918146B2[P]. 2011-04-05.

[24] ZHU Zengbao, XU Rui, LIUChun, et al. Influence of eccentiricity error on the equal load characteristics of a new planetary gear train[J]. Journal of Anhui University of Science and Technology (Natural Science), 2019, 39(6):6-12.

[25] BU Zhonghong, LIU Geng, WU Liyan, et al. A modified approach to deter mine the mesh stiffness and load distribution of cylinder gear based on linear programming[J]. Mechanical and Science and Technology for Aerospace Engineering, 2008, 27(11):1365-1368.